Supporting Information

CO_2/NO_x storage and reduction (CNSR) technology — a new concept for flue gas treatment

Jiaqi Wei [1,2], Yanshan Gao[1,2,*], Cheng Zhang [1,2], Qiang Wang[1,2,*]

[1] College of Environmental Science and Engineering, Beijing Forestry University, Beijing 100083, China

[2] State Key Laboratory of Efficient Production of Forest Resources, Beijing Forestry University, Beijing 100083, China

*Corresponding authors:

Associate Professor Yanshan Gao (E-mail: yanshan_gao@bjfu.edu.cn)

Professor Qiang Wang (E-mail: qiangwang@bjfu.edu.cn)

Calculation formula

The NO_x storage capacity (NSC) in the storage period, as well as NH_3, N_2O, NO_x-des, and N_2 yield during the hydrogenation period, were calculated using Eqs. (S1)-(S5). The CH_4, CO, desorbed CO_2 yield during the hydrogenation period and CO_2 adsorption capacity (C_{CO2}) were calculated using Eqs. (S6)-(S9). The N_2 production was calculated based on the principle of material balance, due to the limitation of N_2 detection by the MKS-2000 instrument. Additionally, the NO_x storage efficiency (NSE) was calculated using Eq. (S10).

$$\text{NSC } (\mu\text{mol g}^{-1}) = \frac{\int_{t_1}^{t_2} (NO_{x\,in} - NO_{x\,out})dt \times F_w \times 10^{-3}}{22.4m} \tag{S1}$$

$$Y_{NH_3} (\mu\text{mol g}^{-1}) = \frac{\int_{t_3}^{t_4} NH_3(t)dt \times F_w \times 10^{-3}}{22.4m} \tag{S2}$$

$$Y_{N_2O} (\mu\text{mol g}^{-1}) = \frac{\int_{t_3}^{t_4} N_2O(t)dt \times F_w \times 10^{-3}}{22.4m} \tag{S3}$$

$$Y_{NO_{x-des}} (\mu\text{mol g}^{-1}) = \frac{\int_{t_3}^{t_4} NO_x(t)dt \times F_w \times 10^{-3}}{22.4m} \tag{S4}$$

$$Y_{N_2} (\mu\text{mol g}^{-1}) = \frac{NO_{x-s} - Y_{NO_{x-des}} - Y_{NH_3} - 2Y_{N_2O}}{2} \tag{S5}$$

$$Y_{CH_4} (\mu\text{mol g}^{-1}) = \frac{\int_{t_3}^{t_4} CH_4(t)dt \times F_w \times 10^{-3}}{22.4m} \tag{S6}$$

$$Y_{CO}\ (\mu mol\ g^{-1}) = \frac{\int_{t_3}^{t_4} CO(t)dt \times F_w \times 10^{-3}}{22.4m} \tag{S7}$$

$$Y_{CO_{2-des}}\ (\mu mol\ g^{-1}) = \frac{\int_{t_3}^{t_4} CO_2(t)dt \times F_w \times 10^{-3}}{22.4m} \tag{S8}$$

$$C_{CO_2}(\mu mol\ g^{-1}) = Y_{CO_{2-des}} + Y_{CH_4} + Y_{CO} \tag{S9}$$

$$NSE(\%) = \frac{\int_{t1}^{t2} (NO_{x,\ in} - NO_{x,\ out})dt}{\int_{t1}^{t2} NO_{x,\ in}dt} \times 100\% \tag{S10}$$

Where t_1 and t_2 (min) are the beginning and ending times of the adsorption period, while t_3 and t_4 are the beginning and ending times of the hydrogenation period, respectively. F_w refers to total flow rate (200 mL min^{-1}) of experimental gases. m is the mass of materials (0.3 g) and 22.4 represents the molar volume of gas (L mol^{-1}).

Table S1 The specific surface area (S_{BET}), pore volume (V_p) and average pore size (d_p) of synthesized $Ni_3Al_1O_x$, $Pt/Ni_3Al_1O_x$, $K\text{-}Pt/Ni_3Al_1O_x$ and $K\text{-}Pt/Ni_3Al_1O_x\text{-}R$ samples.

Sample	S_{BET} ($m^2\ g^{-1}$)	Pore Volume ($cm^3\ g^{-1}$)			Pore Radius (Å)
		V_{total}	V_{micro}	V_{meso}	
$Ni_3Al_1O_x$	180	0.601	0.076	0.525	66.8
$Pt/Ni_3Al_1O_x$	190.9	0.736	0.082	0.654	77.1
$K\text{-}Pt/Ni_3Al_1O_x$	131.1	0.525	0.057	0.468	80
$K\text{-}Pt/Ni_3Al_1O_x\text{-}R$	50.8	0.460	0.028	0.432	181.4

Table S2 H_2 consumption obtained by H_2-TPR.

Sample	H_2 Consumption[a] (mmol g^{-1})
$Ni_3Al_1O_x$	5.45
$Pt/Ni_3Al_1O_x$	5.51
$K\text{-}Pt/Ni_3Al_1O_x$	5.96

[a]Calculated based on H_2-pulse results

Table S3 The summary of integrated CO_2 capture and methanation (ICCM) performance.

Samples	Adsorption conditions	Methanation conditions	CO_2 Uptake (μmol g^{-1})	CO_2 Conv. (%)	CH_4 Sel. (%)	CH_4 Yield (μmol g^{-1})	Cycle	Ref.
0.5%Ni/CeO_2-CaO (0.3 g)	15%CO_2/N_2, 50 mL min^{-1}, 60 mins, T=650 °C	Pure H_2, 50 mL min^{-1}, 60 mins, T=650 °C	–	50.4	85.8	1540 mmol g^{-1} Ni	–	[1]
10Na_2CO_3-10Ni/Al_2O_3 (1 g)	10%CO_2/Ar, 1200 mL min^{-1}, 1 min, T=400 °C	10% H_2/Ar, 1200 mL min^{-1}, 2 mins, T=400 °C	210	–	–	185	20	[2]
10% Ni-6.1% Na_2O/Al_2O_3 (1 g)	7.5%CO_2/N_2, 100 mL min^{-1}, 20 mins, T=320 °C	15%H_2/N_2, 200 mL min^{-1}, 1 h, T=320 °C	389.2	71	–	276.2	–	[3]
5% Ru-6.1% Na_2O/Al_2O_3 (1 g)	7.5%CO_2/4.5% O_2/15% H_2O/N_2, 100 mL min^{-1}, 20 mins, T=320 °C	15%H_2/N_2, 200 mL min^{-1}, 1 h, T=320 °C	393.5	75	–	291.1	–	[3]
4%Ru-8%Na_2CO_3-8%CaO/γ-Al_2O_3 (1 g)	1.5%CO_2/Ar, 1200 mL min^{-1}, 1 min, T=340 °C	10%H_2/Ar, 1200 mL min^{-1}, 2 mins, T=340 °C	243	–	–	241	7	[4]
4%Ru-8%Na_2CO_3-8%CaO/γ-Al_2O_3 (1 g)	1.5%CO_2/10%O_2/400 ppm NO_x/Ar, 1200 mL min^{-1}, 1 min, T=340 °C	10%H_2/Ar, 1200 mL min^{-1}, 2 mins, T=340 °C	209	–	–	196	–	[4]
Ru10CaO/Al_2O_3 (1 g)	1.4%CO_2/Ar, 1200 mL min^{-1}, 1 min, T=370 °C	10%H_2/Ar, 1200 mL min^{-1}, 2 mins, T=370 °C	337	81.3	99.3	272	15	[5]
Ru10Na_2CO_3/Al_2O_3 (1 g)	1.4%CO_2/Ar, 1200 mL min^{-1}, 1 min, T=370 °C	10%H_2/Ar, 1200 mL min^{-1}, 2 mins, T=370 °C	420	95.6	99	398	15	[5]
Ni/AlCaO_x (0.8 g)	10%CO_2/N_2, 400 mL min^{-1}, 5 mins, T=450 °C	30%H_2/N_2, 400 mL min^{-1}, T=450 °C	1796	–	–	1790	10	[6]

$NaNO_3$-Ni/MgO-100-450 (0.5 g)	65%CO_2/N_2, 200 mL min^{-1}, 15 mins, T=450 ^oC	50%H_2/N_2, 200 mL min^{-1}, T=450 ^oC	4580	–	–	910	5	7
NiRu-CaO/CeO_2-Al_2O_3 (0.25 g)	6.44%CO_2/1.10%O_2/2.47% H_2O/N_2, 45 mL min^{-1}, 15 mins, T=350 ^oC	10%H_2/N_2, 45 mL min^{-1}, 15 mins, T=350 ^oC	–	–	100	105	8	8
Ni/Ca(3)/HAP (1 g)	10%CO_2/Ar, 1200 mL min^{-1}, 1 min, T=400 ^oC	10%H_2/N_2, 1200 mL min^{-1}, 2 mins, T=400 ^oC	157.5	–	–	155	–	9
Ni/Ca(3)/HAP (1 g)	10%CO_2/10%O_2/Ar, 1200 mL min^{-1}, 1 min, T=400 ^oC	10%H_2/N_2, 1200 mL min^{-1}, 2 mins, T=400 ^oC	–	–	–	105	5	9
Na-Ru/Al_2O_3 (2.3 cm^3)	5%CO_2/0.25%O_2/1%H_2O/N_2, 20 Sl h^{-1}, 18 mins, T=300 ^oC	15%H_2/N_2, 20 Sl h^{-1}, 14 mins, T=300 ^oC	259	89.1	99.73	183	4	10
Li-Ru/Al_2O_3 (0.6 cm^3)	5%CO_2/0.25%O_2 /N_2, 20 Sdm^3 h^{-1}, 18 mins, T=260 ^oC	15%H_2/N_2, 20 Sdm^3 h^{-1}, 14 mins, T=260 ^oC	295 μmol cm^{-3}	94	–	189 μmol cm^{-3}	3	11
Ru-Ba/Al_2O_3 (0.06 g)	1%CO_2/He, 100 mL (STP) min^{-1}, 10 mins, T=350 ^oC	4%H_2/He, 100 mL (STP) min^{-1}, 10 mins, T=350^oC	–	–	>98	153	3	12
K-Pt/$Ni_3Al_1O_x$ (0.3g)	5%CO_2/5%O_2/Ar, 200 mL min^{-1}, 5 mins, T=350^oC	25%H_2/Ar, 200 mL min^{-1}, 15 mins, T=350 ^oC	–	63.9	97.4	359.5	–	This work
K-Pt/$Ni_3Al_1O_x$ (0.3 g)	5%CO_2/500ppmNO_x/5%O_2/Ar, 200 mL min^{-1}, 3 mins, T=350 ^oC	25%H_2/Ar, 200 mL min^{-1}, 5 mins, T=350 ^oC	–	66.2	>90	194.8	10	This work

Table S4 The CO_2 capture capacity in 10-cycle CNSR test.

Cycle number	1	2	3	4	5	6	7	8	9	10
C_{CO2}[a] (μmol g^{-1})	527.9	299.2	304.5	319.1	316.6	328.5	327.6	323.9	323.3	322.6

[a] CO_2 capture capacity, calculated by Eq. (S9)

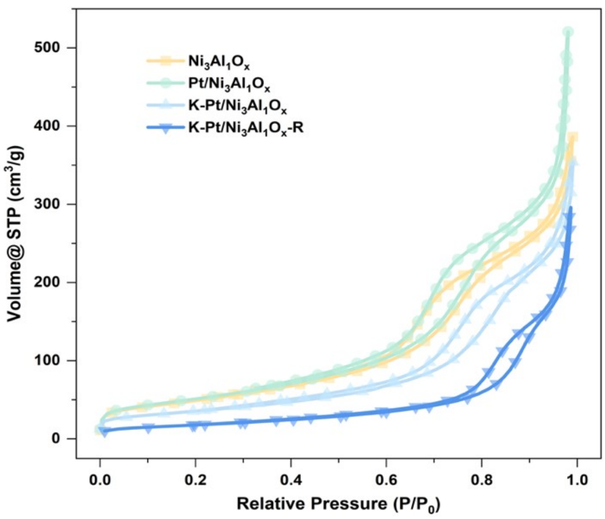

Fig. S1. N_2 adsorption and desorption isotherms of the prepared samples.

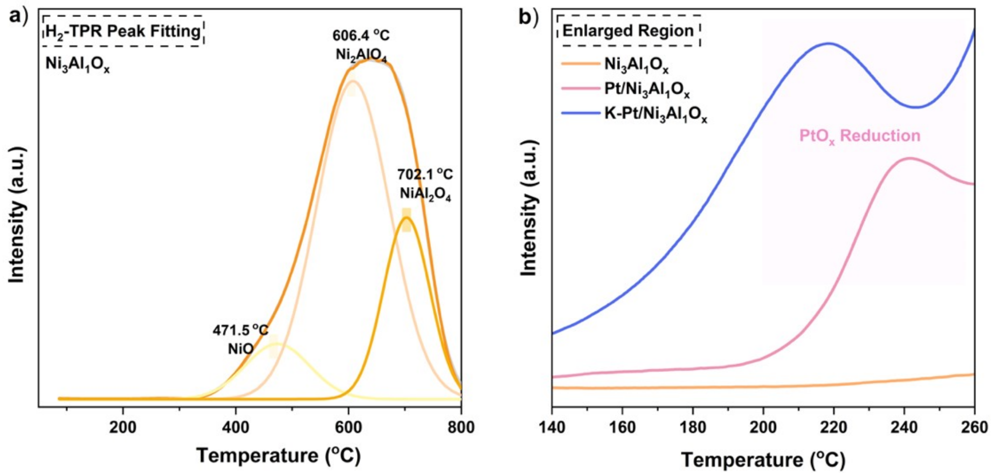

Fig. S2. (a) Deconvoluted H_2-TPR traces (Gaussian peaks) obtained for $Ni_3Al_1O_x$ samples, (b) H_2-TPR analyses of $Ni_3Al_1O_x$, Pt/$Ni_3Al_1O_x$, and K-Pt/$Ni_3Al_1O_x$ samples between 140 °C-260 °C.

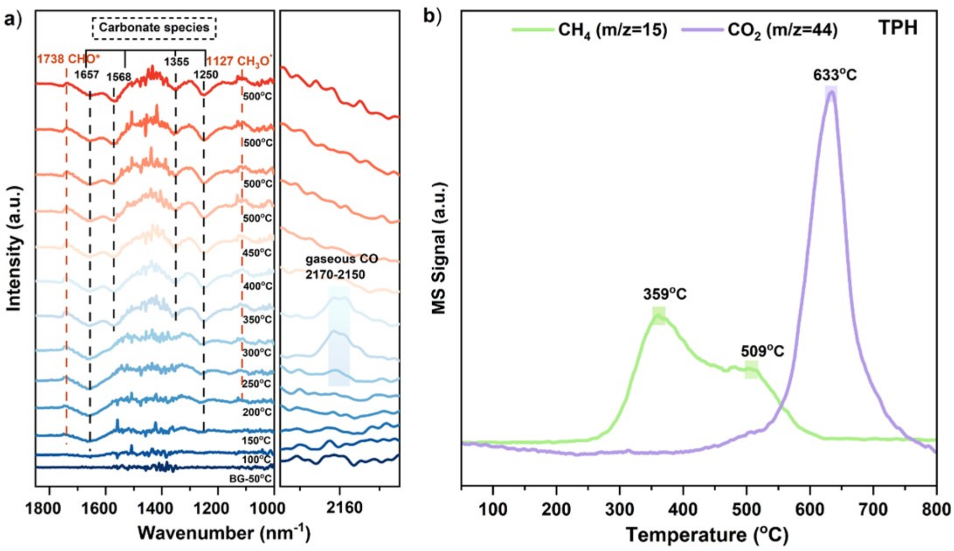

Fig. S3. (a) Temperature-dependent *in situ* DRIFT spectra of the pretreatment process and (b) CH_4 and CO_2 transient curve during TPH process for K-Pt/$Ni_3Al_1O_x$.

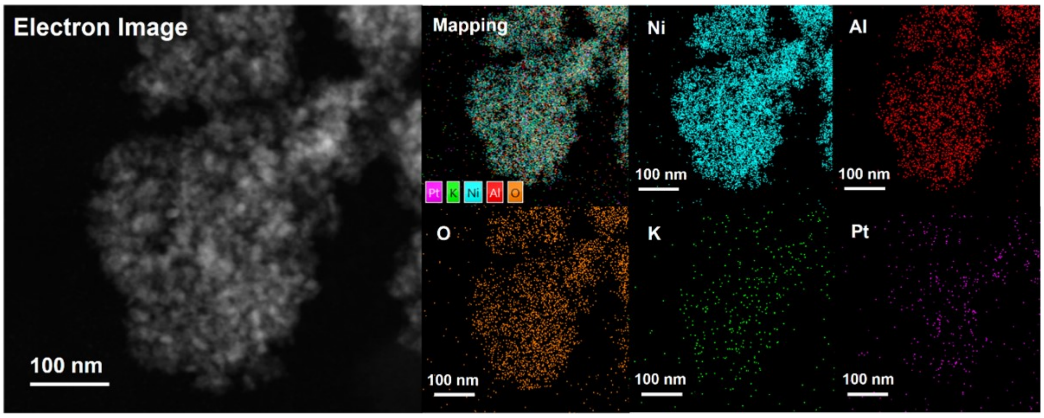

Fig. S4. TEM image and element distribution of Ni, Al, O, K, and Pt for K-Pt/$Ni_3Al_1O_x$-R sample.

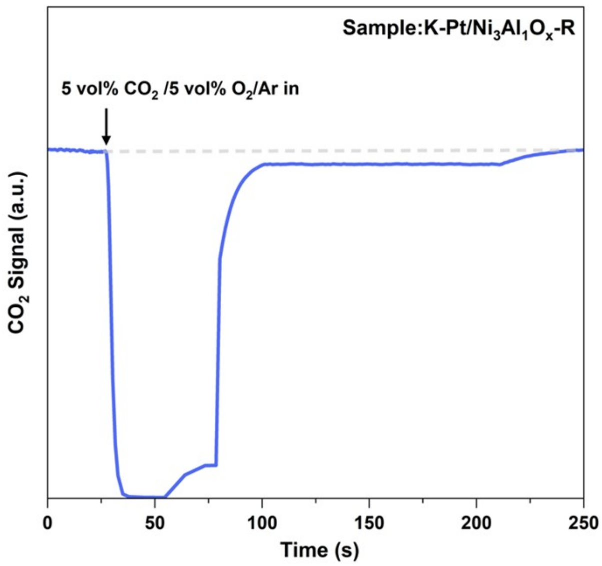

Fig. S5. 5% CO_2 breakthrough curve of K-Pt/$Ni_3Al_1O_x$-R.

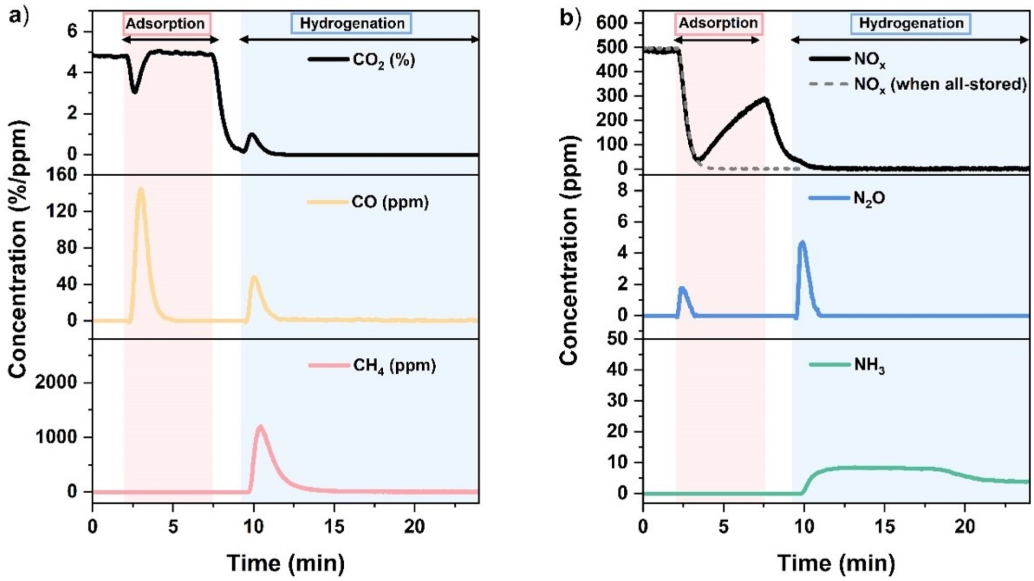

Fig. S6. Instantaneous concentration profiles of each gaseous component: (a) C-species and (b) N-species during CNSR process for the $Pt/Ni_3Al_1O_x$ sample.

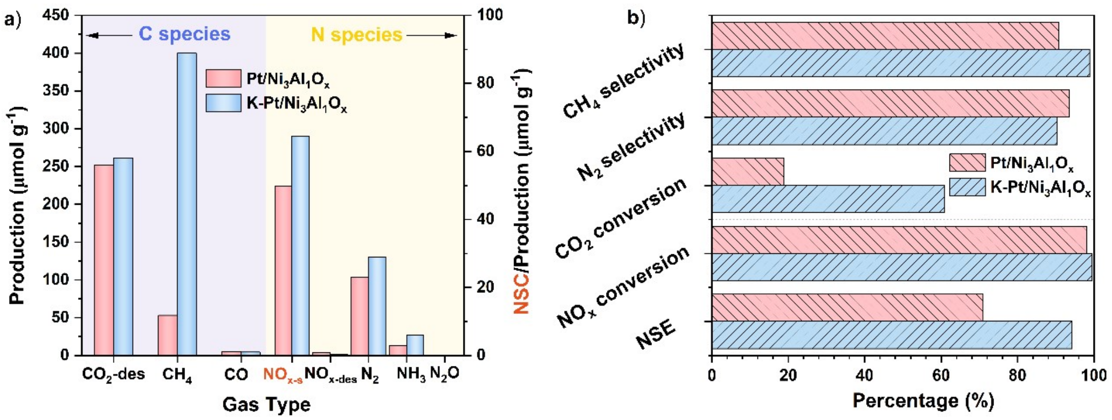

Fig. S7. Performance comparison between Pt/$Ni_3Al_1O_x$ and K-Pt/$Ni_3Al_1O_x$ samples: (a) storage capacity/production and (b) NO_x storage efficiency (NSE), CO_2, NO_x conversion, and CH_4 and N_2 selectivity.

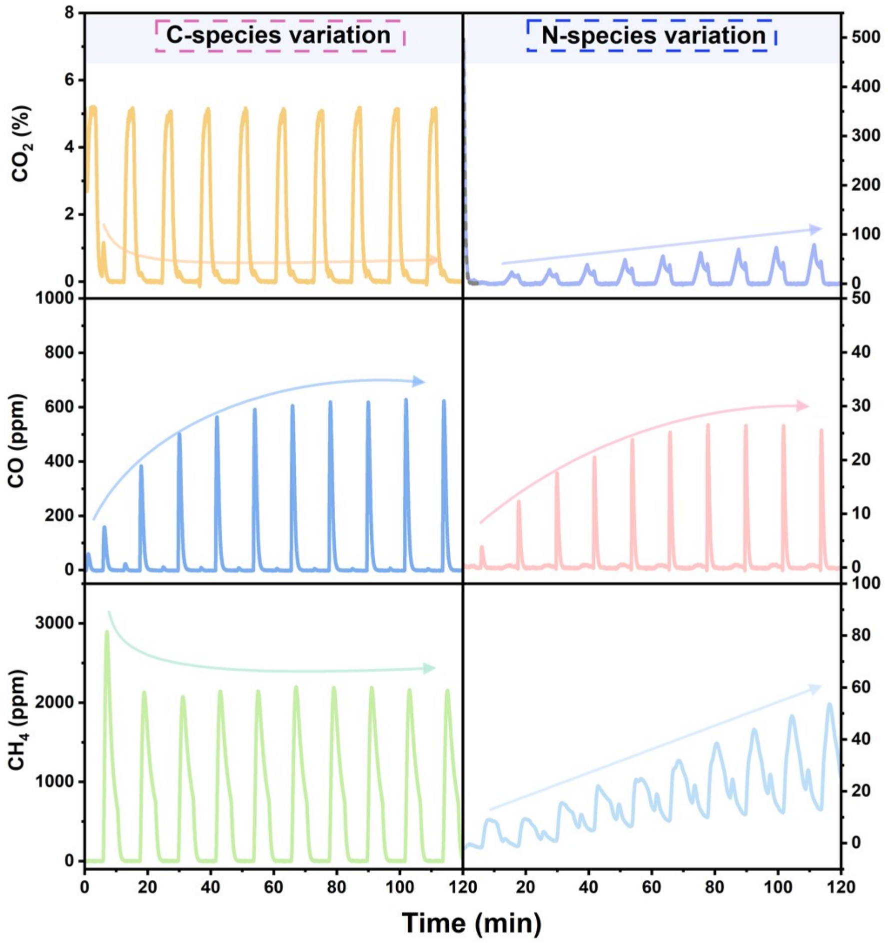

Fig. S8. The dynamic concentration curves of the involved gases over 10 cycles for K-Pt/$Ni_3Al_1O_x$ sample.

Reference

1. H. Sun, Y. Zhang, C. Wang, M. A. Isaacs, A. I. Osman, Y. Wang, D. Rooney, Y. Wang, Z. Yan, C. M. A. Parlett, F. Wang and C. Wu, *Chemical Engineering Journal*, 2022, **437**, 135394.
2. A. Bermejo-Lopez, B. Pereda-Ayo, J. A. Gonzalez-Marcos and J. R. Gonzalez-Velasco, *Journal of CO_2 Utilization*, 2019, **34**, 576-587.
3. M. A. Arellano-Trevino, Z. He, M. C. Libby and R. J. Farrauto, *Journal of CO_2 Utilization*, 2019, **31**, 143-151.
4. A. Bermejo-López, B. Pereda-Ayo, J. A. Onrubia-Calvo, J. A. González-Marcos and J. R. González-Velasco, *Journal of CO_2 Utilization*, 2023, **67**, 102343.
5. A. Bermejo-López, B. Pereda-Ayo, J. A. González-Marcos and J. R. González-Velasco, *Applied Catalysis B: Environmental*, 2019, **256**, 117845.
6. L. Li, Y. Zhang, J. Feng, S. Zhao, K. Li, Z. Huang and H. Lin, *ACS Sustainable Chemistry & Engineering*, 2024, **12**, 925-937.
7. P. Huang, J. Chu, J. Fu, J. Yu, S. Li, Y. Guo, C. Zhao and J. Liu, *Chemical Engineering Journal*, 2023, **467**, 143431.
8. L.-P. Merkouri, L. F. Bobadilla, J. L. Martín-Espejo, J. A. Odriozola, A. Penkova, G. Torres-Sempere, M. Short, T. R. Reina and M. S. Duyar, *Applied Catalysis B: Environment and Energy*, 2025, **361**, 124610.
9. Z. Boukha, A. Bermejo-López, U. De-La-Torre and J. R. González-Velasco, *Applied Catalysis B: Environmental*, 2023, **338**, 122989.
10. S. Cimino, E. M. Cepollaro and L. Lisi, *Applied Catalysis B: Environmental*, 2022, **317**, 121705.
11. S. Cimino, E. M. Cepollaro, M. Pazzi and L. Lisi, *Catalysis Today*, 2024, **426**, 114366.
12. A. Porta, C. G. Visconti, L. Castoldi, R. Matarrese, C. Jeong-Potter, R. Farrauto and L. Lietti, *Applied Catalysis B: Enviromental*, 2021, **283**, 119654.